Temperature-Dependent Pulsed Electron Paramagnetic Resonance Studies of the S_2 State Multiline Signal of the Photosynthetic Oxygen-Evolving Complex†

Gary A. Lorigan and R. David Britt*

Department of Chemistry, University of California, Davis, Davis, California 95616

Received June 8, 1994; Revised Manuscript Received August 1, 1994®

ABSTRACT: The electron spin–lattice relaxation rate ($1/T_1$) of the $g = 2$ "multiline" manganese electron paramagnetic resonance (EPR) signal arising from the photosystem II oxygen-evolving complex poised in the S_2 state has been directly measured over the temperature range of 4.2–11 K via the inversion–recovery pulsed EPR technique. The electron spin echo amplitude of the $g = 2$ "multiline" signal varies inversely with temperature over this range, indicating a ground spin state Curie law behavior in agreement with our previously reported work [Britt et al. (1992) *Biochim. Biophys. Acta 1140*, 95–101]. Results of a plot of the natural log of the electron spin–lattice relaxation rate versus reciprocal temperature are consistent with an Orbach mechanism serving as the dominant relaxation pathway for the "multiline" signal in this temperature range. The slope of the plot indicates that an excited spin state manifold exists 36.5 cm^{-1} above the ground-state manifold that gives rise to the "multiline" signal.

Higher plant photosynthesis evolves O_2 through a cyclic water oxidation process occurring in the oxygen-evolving complex (OEC)[1] of photosystem II (PSII). This cycle (Kok et al., 1970), involves five states, S_0–S_4, where the subscript represents the net oxidized state of the OEC. States S_1–S_4 are produced by sequential single-electron oxidations of the OEC by the photogenerated P_{680}^+ cation. The tyrosine residue Y_Z serves as an electron transfer intermediate in each transition (Barry & Babcock, 1987; Debus et al., 1988). Molecular oxygen is spontaneously released from the OEC after the S_4 state is generated, and the OEC resets to the S_0 state as it is rereduced by four electrons from the two oxidized substrate water molecules. The net result of the cycle is the release of an oxygen molecule and the transfer of the four electrons to the quinone electron acceptor molecules of PSII. The detailed structure of the OEC has not been determined, but electron paramagnetic resonance (EPR) studies have demonstrated that the OEC contains a tetranuclear Mn cluster (Kim et al., 1990, 1992; Zimmermann & Rutherford, 1986; Brudvig, 1989, 1994; Bonvoisin, 1992). The cluster is coordinated by at least one protein histidine ligand (Tang et al., 1994).

When the OEC of PSII is poised in the S_2 state of the Kok cycle, EPR signals arise in the $g = 2$ and $g = 4.1$ regions of the spectrum (Sauer et al., 1992; Rutherford et al., 1991, 1992; Babcock, 1987; Debus, 1992; Dismukes & Siderer, 1981). The $g = 2$ EPR signal, commonly referred to as the "multiline" signal, is composed of at least 19 partially resolved Mn hyperfine lines with an average splitting of approximately 80 G (Dismukes & Siderer, 1981). The 360-G wide $g = 4.1$ EPR signal does not reveal any hyperfine structure in nonoriented PSII membranes (Casey & Sauer, 1984; Zimmermann & Rutherford, 1984), but oriented NH_3-treated membranes display at least 16 Mn hyperfine lines with an average splitting of approximately 36 G (Kim et al., 1990, 1992). The first two continuous wave (CW) EPR power saturation studies on the multiline signal indicated that the signal arises from a low-lying excited spin state (de Paula & Brudvig, 1985; de Paula et al., 1986), but now both pulsed and CW EPR studies have shown that the signal arises from an $S = {}^1/_2$ ground spin state (Britt et al., 1992; Hansson et al., 1987; Pace et al., 1991). The $g = 2$ multiline and $g = 4.1$ EPR signals are believed to arise from two different isolated spin states of an exchange-coupled tetranuclear Mn cluster (Kim et al., 1990, 1992; Zimmermann & Rutherford, 1986; Brudvig, 1989; Bonvoisin, 1992).

This work investigates spin–lattice relaxation of electron magnetization of this Mn cluster when poised in the state giving rise to the $g = 2$ multiline signal. The electron spin–lattice (or longitudinal) relaxation time T_1 is the time constant for relaxation of electronic magnetization along the axis parallel with the static magnetic field. The electron spin–lattice relaxation rate $1/T_1$ constitutes the rate at which energy is exchanged between the spin system and the lattice. In the solid state, electron spin-lattice relaxation occurs through a coupling of the electron spins to phonon vibrational lattice modes (Abragam & Bleaney, 1970; Standley & Vaughan, 1969; Banci et al., 1991). The phonon density spectrum of the lattice determines the relaxation mechanism of the spin system by dictating the number of phonons available for relaxation. The Raman and Orbach processes are two common relaxation mechanisms observed at temperatures greater than 2 K. The Raman process proceeds through a "virtual" intermediate by the absorption and emission of two phonons whose energy difference matches the energy difference between electron spin states (Van Vleck, 1940). The entire phonon spectrum can contribute to Raman relaxation. Raman relaxation shows a high power dependence on temperature: $1/T_1 \propto T^x$ ($3 \leq x \leq 9$). If a "real" low-lying excited spin manifold exists about the ground-state manifold, the Orbach process can dominate the relaxation pathway (Orbach, 1961a,b). Given an excited spin manifold at energy Δ above the ground-state manifold, the spin system is promoted into the excited spin manifold by the absorption of a phonon of energy $h\nu \approx \Delta$ and returns to another spin state of the ground state manifold as another phonon of slightly different energy

† R.D.B. acknowledges support from the U.S. Department of Agriculture (NRICGP Grant 92-01413), the National Institutes of Health (Grant BMT 1 R29 GM48242-01), and the Camille and Henry Dreyfus Foundation.

* Address correspondence to this author.

® Abstract published in *Advance ACS Abstracts,* September 15, 1994.

[1] Abbreviations: EPR, electron paramagnetic resonance; CW, continuous wave; OEC, oxygen-evolving complex; PSII, photosystem II; ESE, electron spin echo; EXAFS, extended X-ray absorption fine structure.

0006-2960/94/0433-12072$04.50/0

is emitted. The net process results in a spin transition within the ground-state manifold, and as in the Raman mechanism the phonon energy difference matches the energy difference between electron spin states. However, since only phonons with energy $h\nu \approx \Delta$ contribute to the Orbach relaxation process, a different temperature dependence is observed for the relaxation rate (Orbach, 1961a,b; Weil et al., 1994). For low temperatures such that $k_BT \ll \Delta$, the Orbach relaxation rate varies exponentially with inverse temperature: $1/T_1 \propto \exp(-\Delta/k_BT)$.

In addition to the spin–lattice relaxation, spin–spin (or transverse) relaxation processes occur. The spin–spin relaxation rate $1/T_2$ is the rate at which spins of the same resonant frequency transfer energy among themselves, where T_2 is the time constant for this relaxation of magnetization perpendicular to the static magnetic field.

The temperature dependence of the electron spin–lattice relaxation rate $1/T_1$ of the $g = 2$ multiline signal has been indirectly explored with CW EPR power saturation and line-broadening studies, with the aim of elucidating the relaxation mechanism of the spin system. In a power saturation study, the amplitude A of an EPR signal varies with microwave power P as $A = K\sqrt{P}(1 + P/P_{1/2})^{-b/2}$, where K is a spin concentration constant, b is the inhomogeneity parameter, and $P_{1/2}$ is the power at half-saturation at a given temperature (Rupp et al., 1978). A plot of $\log_{10}(A/\sqrt{P})$ vs $\log_{10}(\sqrt{P})$ shows two limiting regimes: the low-power nonsaturating limit presents a straight line collinear with the $\log_{10}(\sqrt{P})$ axis, and the high-power saturating limit presents a straight line with a slope equal to $b/2$. The point at which the projections of the two line bisect reveals the power at half-saturation ($P_{1/2}$), which is proportional to the product of the electron spin–lattice relaxation rate $1/T_1$ and the electron spin–spin relaxation rate $1/T_2$ (Rupp et al., 1978; de Paula & Brudvig, 1985). If one assumes that T_2 is independent of temperature, a $P_{1/2}$ versus temperature plot can be used to infer the temperature dependence of the spin–lattice relaxation rate. However, at sufficiently low temperatures, the $P_{1/2}$ point can be difficult to measure accurately because the signal saturates quite easily, thus inducing a large error in the measurement of $P_{1/2}$. This error coupled with the assumption that T_2 is a constant creates a large uncertainty in the actual temperature dependence of the spin–lattice rate and the corresponding establishment of a relaxation mechanism. It is also possible to address relaxation rate changes by measuring the EPR line widths as a function of temperature. Hansson et al. (1987) measured the lifetime broadening of the multiline signal as a function of temperature and assumed that T_2 is independent of temperature, resulting in a line width assumed proportional to $1/T_1$. Both power saturation and line width analysis studies have favored the Orbach process as the dominant relaxation pathway for the multiline signal. In the various studies the energy difference between the ground and first excited spin state manifolds has been estimated to range from 13 cm^{-1} to 42 cm^{-1} (Hansson et al., 1984, 1987; de Paula & Brudvig, 1985; Pace et al., 1991). The plots that were used in these studies to identify the Orbach process as the dominant relaxation pathway and measure the energy difference between the ground and first excited spin state manifolds have consisted of only three or four experimental data points. Furthermore, some of the experiments were carried out under saturating conditions (Brudvig, 1994). Given the range of results and the difficulties of interpreting these CW EPR measurements, we consider there to be appreciable uncertainty in the measurements of the temperature dependence of the spin–lattice relaxation rate and the subsequent assignment to a specific mechanism.

Pulsed EPR spectroscopy provides a direct measurement of relaxation rates $1/T_1$ and $1/T_2$. In a pulsed experiment, one can accurately measure the relaxation rate by monitoring the magnetization of the spin system on a time scale comparable with relaxation. In this paper, we have utilized the inversion–recovery pulsed EPR technique to directly measure the electron spin–lattice relaxation rate of the multiline signal as a function of temperature. This technique has enabled us to demonstrate that the multiline signal relaxes via the Orbach process and to accurately establish an energy difference of 36.5 cm^{-1} between the ground and first excited spin state manifolds.

EXPERIMENTAL PROCEDURES

Sample Preparation. PSII O_2-evolving membranes were prepared from freshly grown hydroponic spinach with a slightly modified version of the BBY preparation (Berthold et al., 1981) as described in Kim et al. (1992). The final pellet was resuspended in buffer containing 0.4 M sucrose, 5 mM $MgCl_2$, 15 mM NaCl, 5 mM $CaCl_2$, 1 mM EDTA, 50 mM MES at pH 6.0, and 5% ethanol by volume. The PSII membranes were then loaded into 3.8-mm o.d. quartz EPR tubes and primarily poised in the S_1 state by dark adaptation at 273 K for 15 min, followed by immersion into a liquid N_2 dewar at 77 K for storage prior to use. Advancement to S_2 was obtained by illumination at a temperature of 195 K with a 120-V/300-W Radiac IR-filtered light source.

EPR Experiments. X-band CW EPR spectra were obtained with a Bruker ER 200 D spectrometer equipped with an ESR 900 continuous-flow liquid He cryostat and an Oxford Instruments Model ITC4 temperature controller. The temperature was maintained at 7 K. A Macintosh IIci microcomputer with a National Instruments NB-MIO-16-L A/D board interfaced to the spectrometer was utilized to record the spectra.

The pulsed EPR experiments were performed with an instrument of our own design and construction (Sturgeon & Britt, 1992). The electron spin–lattice relaxation rates were measured with an inversion–recovery pulse sequence (π–T–$\pi/2$–τ–π–τ–ESE) (Banci et al., 1991). In this sequence, the first π pulse inverts the electron spin magnetization, while the recovery time T is varied stepwise until the magnetization (which is monitored with the terminal two-pulse Hahn sequence) returns to equilibrium. The two-pulse interpulse time τ was held constant at 210 ns. The repetition delay time between individual pulse sets was adjusted to at least four times the maximal recovery time T to ensure that each pulse set started with the spin system at equilibrium. The temperature was monitored and controlled with a Lake Shore Cryotronics Model 805 temperature controller measuring the resistance of a Lake Shore Cryotronics TG-120P gallium–aluminum–arsenide diode sensor mounted near the sample position of an X-band pulsed EPR probe inserted in the variable-temperature sample chamber of a Janis Supervaritemp liquid He cryostat. (Sturgeon & Britt, 1992; Britt & Klein, 1987). The system stabilizes the temperature at a set value by controlling the temperature of the cold He gas introduced into the sample chamber.

Data Analysis. The amplitude of the two-pulse echo measured at time T in the inversion–recovery sequence is a measure of the time-dependent z component of the magnetization $M_z(T)$ for those spins resonant within the bandwidth of the excitation pulse. The inversion–recovery data were fit

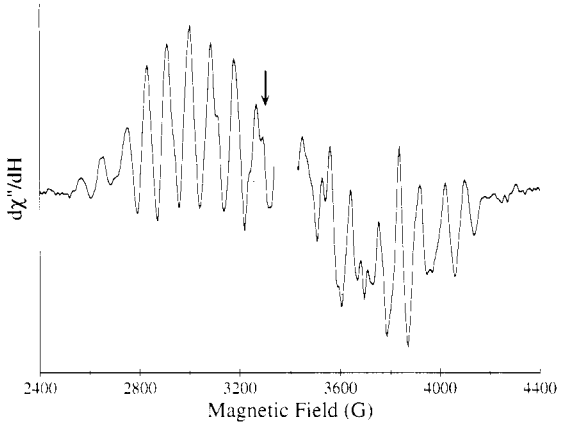

FIGURE 1: CW EPR spectrum of the (illuminated – dark-adapted) $g = 2$ multiline signal obtained from PSII membranes. The spectrum results from the subtraction of the dark-adapted S_1 state from the illuminated S_2 state in order to isolate the signal arising from the $S_1 \rightarrow S_2$ transition. The spectrum was obtained at a modulation amplitude of 20 G pp, a field modulation frequency of 100 kHz, a receiver time constant of 200 ms, a microwave frequency of 9.57 GHz, a microwave power of 2.1 mW, and a temperature of 7 K. The arrow indicates the field position where the inversion–recovery traces of Figure 2 were recorded.

to a single-exponential recovery function according to the Bloch equation result (Bloch, 1946; Poole & Farach, 1971; Banci et al., 1991):

$$M_z(T) = M_0[1 - 2\exp(-T/T_1)] \quad (1)$$

where M_0 is the value of M_z at equilibrium. The single-exponential fits were calculated through a nonlinear regression analysis technique employing the Levenberg–Marquardt algorithm. The standard deviations calculated from the fits are included in the caption to Figure 2 (Press et al., 1989).

RESULTS

Figure 1 shows a typical CW EPR spectrum for the (illuminated – dark-adapted) $g = 2$ "multiline" signal. The $g = 2$ tyrosine radical (signal II) is excised from the spectrum. The ESE-detected field-swept spectrum is comparable to previously reported work (Britt et al., 1992).

Temperature Dependence of the Electron Spin–Lattice Relaxation Rate. Figure 2 displays three selected inversion–recovery traces for the multiline signal (illuminated – dark-adapted) over the temperature range from 4.2 to 11.0 K. The traces in Figure 2 result from the subtraction of the dark-adapted S_1 state data from the illuminated S_2 state data in order to isolate the inversion–recovery of the multiline signal produced upon the $S_1 \rightarrow S_2$ transition. The experimental data points are shown as crosses, while the solid lines represent nonlinear least-squares fits of the experimental data to the single-exponential recovery functioon shown in eq 1. The calculated electron spin–lattice relaxation times and the standard deviations are included in the figure caption. Data were not recorded at temperatures above 11.0 K due to decreased signal-to-noise ratios. We consider the fits to the single-exponential recovery function to be rather good. There may be some deviations due to spectral diffusion contributions (Beck et al., 1991; Smigel et al., 1974; Dalton et al., 1972; Kevan, 1979), but these appear to be minimal in this case. One factor minimizing spectral diffusion in these experiments is the short (≈10 ns) pulse lengths with the correspondingly wide bandwidths. Also, the spin–lattice relaxation rates are relatively fast, particularly at the higher temperatures, and

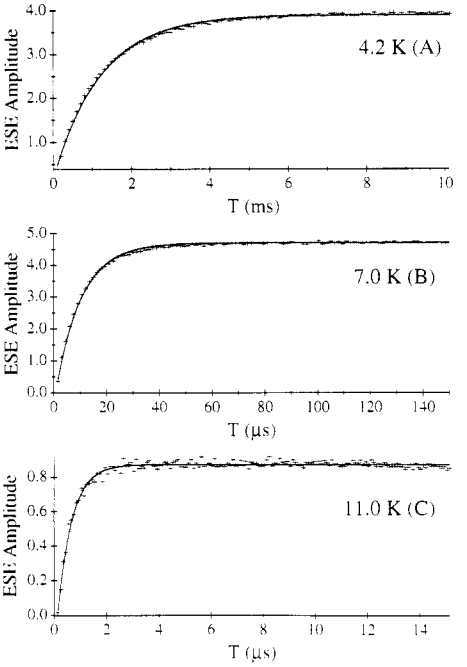

FIGURE 2: Inversion–recovery traces for the (illuminated – dark-adapted) multiline signal. The spectra were obtained with a fixed magnetic field value of 3240 G, a constant interpulse time τ of 210 ns, and a microwave frequency of 9.381 GHz. The repetition time in between pulse trains was set to at least 4 times the maximum recovery time T at each temperature to ensure that the spin system had returned to equilibrium. The experimental data points are shown as crosses, while the solid lines represent a nonlinear least-squares fit of the experimental data to the single-exponential recovery function shown in eq 1. The temperatures and electron spin–lattice relaxation times for the traces shown in the figure are (A) 4.2 K, $T_1 = 1.22 \pm 0.02$ ms; (B) 7.0 K, $T_1 = 9.80 \pm 0.10$ μs; (C) 11.0 K, $T_1 = 0.56 \pm 0.01$ μs. Additional temperature-dependent electron spin–lattice relaxation times measured via the inversion–recovery method but not displayed in the figure are 6.0 K, $T_1 = 38.2 \pm 0.5$ μs; 8.0 K, $T_1 = 3.46 \pm 0.05$ μs; 9.0 K, $T_1 = 1.59 \pm 0.03$ μs; 10.0 K, $T_1 = 0.89 \pm 0.02$ μs.

such fast relaxation will diminish contributions from competing processes.

Figure 3A displays the natural log of the calculated electron spin–lattice relaxation rate of the multiline signal (obtained from Figure 2) plotted versus the natural log of temperature to explore the possibility that the Raman process provides the dominant relaxation pathway, in which case we expect the rate to vary as a high power of the temperature: $1/T_1 \propto T^x$ ($3 \leq x \leq 9$). The data points are shown as diamonds, while the solid line results from a linear least-squares fit of the data. The slope (8.0 ± 0.4) of the graph corresponds to a $T^{8.0\pm0.4}$ Raman power temperature dependence. However, the plot shows consistent curvature; the function does not provide a good linear fit to the data. The residuals of the data displayed at the bottom of the figure clearly show this nonlinear behavior over the entire temperature range, where the experimental data points are not randomly scattered above and below the fit. Specifically, the lowest temperature point falls below the straight-line fit and as the temperature is increased the data start to fall above the fit until near the highest temperature point where it once again falls below the fit.

The natural log of the calculated electron spin–lattice relaxation rates obtained from the multiline traces in Figure 2 is plotted versus reciprocal temperature in Figure 3B. This graph explores the alternate possibility that the Orbach process provides the dominant relaxation pathway, in which case we expect the rate to vary exponentially with inverse tempera-

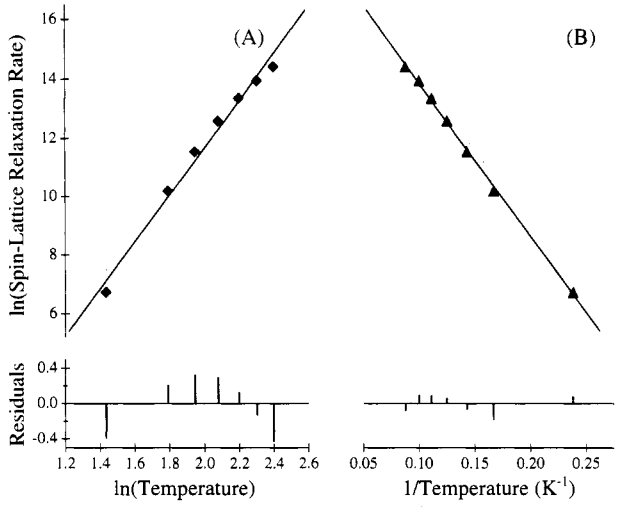

FIGURE 3: (A) Raman plot displaying the natural log of the electron spin–lattice relaxation rate of the magnetization giving rise to the multiline EPR signal as a function of the natural log of the temperature. The experimental data points are represented by diamonds, while the solid line represents a least-squares linear fit of the data. The slope of the linear fit is 8.0 ± 0.4, corresponding to a $T^{8\pm0.4}$ Raman power temperature dependence. (B) Orbach plot displaying the natural log of the electron spin–lattice relaxation rate of the magnetization giving rise to the multiline EPR signal as a function of reciprocal temperature. The solid line represents a linear least-squares fit of the experimental data with a slope of −52.1 ± 0.9. This slope corresponds to a energy difference (Δ) of 36.5 ± 0.7 cm^{-1} between the ground and first excited spin state manifolds. The experimental data points shown as triangles were obtained from the single-exponential recovery T_1 fits such as illustrated in Figure 2. The residuals of the data shown at the bottom of each plot were obtained by subtracting the linear fit from the experimental data points.

ture: $1/T_1 \propto exp(-\Delta/k_BT)$. The experimental data points are shown as triangles, while the solid line represents a linear least-squares fit of the data. The straight-line fit of this data to the Orbach relaxation function is excellent, particularly in contrast to the poor straight-line fit of Figure 3A. The residuals in Figure 3B clearly emphasize this point, where the experimental data points are closely scattered above and below the linear fit. The excellent straight-line fit of this data provides strong support to the assignment of the Orbach mechanism as the major route for spin–lattice relaxation of the unpaired spins of the cluster. The slope of the graph is equal to −52.1 ± 0.9, corresponding to a energy difference (Δ) between the ground and first excited spin state manifolds of 36.5 ± 0.7 cm^{-1}.

Ground-State Curie Low Behavior. The equilibrium magnetization of an isolated ground spin manifold varies inversely with temperature in the regime where $g\beta H \ll k_BT$. Figure 4 plots the ESE amplitude at the maximum recovery time T versus inverse temperature for the traces in Figure 2. From the form of the inverse recovery function (eq 1) we note that to very good approximation the magnetization will return to its equilibrium value by a recovery time 5 times greater than T_1 (Banci et al., 1991). In these data sets the maximum recovery times are at least 8 times longer than the corresponding T_1 values. The experimental data points are shown as circles, while the solid line results from a linear least-squares fit of the data. The trace obtained at 4.2 K was omitted from the graph because the sample was immersed in liquid He, thus causing a slight shift in the resonant microwave frequency which in turn induces a change in the echo amplitude of the signal. The linear plot indicates that the multiline signal follows ground-state Curie law behavior over this temperature

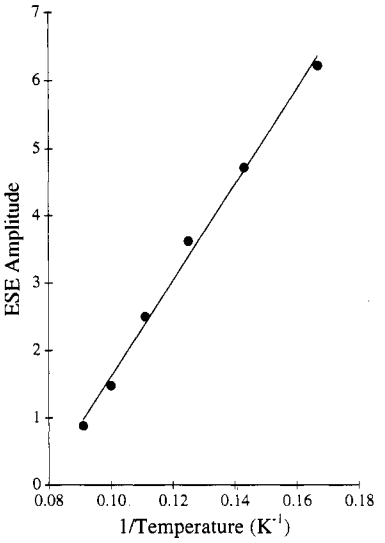

FIGURE 4: Plot of the ESE amplitude at the maximum recovery time T versus inverse temperature from the multiline traces such as illustrated in Figure 2. The experimental data points are shown as circles, while the solid line represents a least-squares linear fit of the data. The linear plot illustrates the ground-state Curie law behavior of the multiline signal.

range. This is consistent with our previous pulsed EPR study carried out at lower temperatures (Britt et al., 1992).

DISCUSSION

For EPR experiments performed at X-band frequencies (≈10 GHz), the dominant relaxation pathway at temperatures below approximately 2 K involves the direct absorption or emission of energy via the interaction of a spin with a single phonon. However, at higher temperatures, the vast majority of the phonon spectral density function occurs at frequencies higher than the resonant microwave frequency. At such temperatures the two-phonon Raman process dominates over the direct one-phonon interaction. However, if additional spin state manifolds are thermally accessible in a spin system, the Orbach two-phonon mechanism may provide for faster relaxation than the Raman process. Our temperature-dependent spin–lattice relaxation measurements indicate that this is indeed the case for the Mn cluster of PSII poised in the S_2 state of the Kok cycle. The results indicate the presence of an excited spin state manifold 36.5 cm^{-1} above the ground spin state manifold that gives rise to the $g = 2$ multiline EPR signal. Our value of 36.5 cm^{-1} is in closest agreement with the approximate value of 30 cm^{-1} obtained via both progressive microwave power saturation and temperature-dependent line width studies by Hansson et al. (1984, 1987). The excited spin state manifold lies much lower in energy than the excited spin state manifolds in dinuclear mixed-valence Mn compounds that have the same 2.7-Å Mn–Mn distance determined from extended X-ray absorption fine structure (EXAFS) to be present in the PSII Mn cluster (Sauer et al., 1992). In such Mn(III)Mn(IV) clusters, the typical value of the exchange interaction is 300 cm^{-1}, placing the first excited spin state manifold at an energy 450 cm^{-1} above the ground-state manifold (Brudvig, 1989). Our inversion–recovery measurements of the temperature dependence of the spin–lattice relaxation rate thus reveal a further spectroscopic dissimilarity between the OEC Mn cluster and these mixed-valence dinuclear Mn complexes. Excited spin state manifolds at relatively low energy would indeed be expected for a higher nuclearity cluster due to the increased density of spin state

manifolds resulting from the magnetic coupling of more paramagnetic ions (de Paula & Brudvig, 1985; de Paula et al., 1986; Brudvig, 1989).

REFERENCES

Abragam, A., & Bleaney, B. (1970) *Electron Paramagnetic Resonance of Transition Ions*, Clarendon, Oxford, England.

Babcock, G. T. (1987) in *Photosynthesis: New Comprehensive Biochemistry* (Amesz, J., Ed.) 15th ed., pp 125–158, Elsevier, Amsterdam.

Banci, L., Bertini, I., & Luchinat, C. (1991) *Nuclear and Electron Relaxation*, VCH, New York.

Barry, B. A., & Babcock, G. T. (1987) *Proc. Natl. Acad. Sci. U.S.A. 84*, 7099–7103.

Beck, W. F., Innes, J. B., Lynch, J. B., & Brudvig, G. W. (1991) *J. Magn. Reson. 91*, 12–29.

Berthold, D. A., Babcock, G. T., & Yocum, C. F. (1981) *FEBS Lett. 134*, 231–234.

Bloch, F. (1946) *Phys. Rev. 70*, 460–474.

Bonvoisin, J., Blondin, G., Girerd, J. J., & Zimmermann, J.-L. (1992) *Biophys. J. 61*, 1076–1086.

Britt, R. D., & Klein, M. P. (1987) *J. Magn. Reson. 74*, 535–540.

Britt, R. D., Lorigan, G. A., Sauer, K., Klein, M. P., & Zimmermann, J.-L. (1992) *Biochim. Biophys. Acta 1140*, 95–101.

Brudvig, G. W. (1989) in *Advanced EPR Applications in Biology and Biochemistry* (Hoff, A. J., Ed.) pp 839–863, Elsevier, Amsterdam.

Brudvig, G. W. (1994) in *Mechanistic Bioinorganic Chemistry* (Thorp, H., & Pecoraro, V. L., Eds.) American Chemical Society, Washington, DC.

Casey, J. L., & Sauer, K. (1984) *Biochim. Biophys. Acta 767*, 21–28.

Dalton, L. R., Kwiram, A. L., & Cowen, J. A. (1972) *Chem. Phys. Lett. 17*, 495–499.

Debus, R. J. (1992) *Biochim. Biophys. Acta 1102*, 269–352.

Debus, R. J., Barry, B. A., Babcock, G. T., & McIntosh, L. (1988) *Proc. Natl. Acad. Sci. U.S.A. 85*, 427–430.

de Paula, J. C., & Brudvig, G. W. (1985) *J. Am. Chem. Soc. 107*, 2643–2648.

de Paula, J. C., Beck, W. F., & Brudvig, G. W. (1986) *J. Am. Chem. Soc. 108*, 4002–4009.

Dismukes, G. C., & Siderer, Y. (1981) *Proc. Natl. Acad. Sci. U.S.A. 78*, 274–278.

Hansson, Ö., Andréasson, L.-E., & Vänngård, T. (1984) in *Advances in Photosynthesis Research* (Sybesma, C., Ed.), Vol. I, pp 307–310, Nijhoff and Junk, The Hague, The Netherlands.

Hansson, Ö., Aasa, R., & Vänngård, T. (1987) *Biophys. J. 51*, 825–832.

Kevan, L. (1979) in *Time Domain Electron Spin Resonance* (Kevan, L., & Schwartz, R. N., Eds.) pp 279–341, Wiley, New York.

Kim, D. H., Britt, R. D., Klein, M. P., & Sauer, K. (1990) *J. Am. Chem. Soc. 112*, 9389–9391.

Kim, D. H., Britt, R. D., Klein, M. P., & Sauer, K. (1992) *Biochemistry 31*, 541–547.

Kok, B., Forbush, B., & McGloin, M. (1970) *Photochem. Photobiol. 11*, 457–475.

Orbach, R. (1961a) *Proc. R. Soc. London, Ser. A 264*, 458–484.

Orbach, R. (1961b) *Proc. R. Soc. London, Ser. A 264*, 485–495.

Pace, R. J., Smith, P., Bramley, R., & Stehlik, D. (1991) *Biochim. Biophys. Acta 1058*, 161–170.

Poole, C. P., & Farach, H. A. (1971) *Relaxation in Magnetic Resonance*, Academic Press: New York.

Press, W. H., Flannery, B. P., Teukolsky, S. A., & Vetterling, W. T. (1989) *Numerical Recipes in C*, Cambridge Univ. Press, Cambridge, England.

Rupp, H., Rao, K. K., & Cammack, R. (1978) *Biochim. Biophys. Acta 537*, 255–269.

Rutherford, A. W., Boussac, A., & Zimmermann, J.-L. (1991) *New J. Chem. 15*, 491–500.

Rutherford, A. W., Zimmermann, J.-L., & Boussac, A. (1992) in *The Photosystems: Structure, Function and Molecular Biology* (Barber, J., Ed.) pp 179–229, Elsevier, Amsterdam.

Sauer, K., Yachandra, V. K., Britt, R. D., & Klein, M. P. (1992) in *Manganese Redox Enzymes* (Pecoraro, V. L., Ed.) pp 141–175, VCH, New York.

Smigel, M. D., Dalton, L. A., & Dalton, L. R. (1974) *Chem. Phys. 6*, 183–192.

Standley, K. J., & Vaughan, R. A. (1969) *Electron Spin Relaxation Phenomena in Solids*, Plenum, New York.

Sturgeon, B. E., & Britt, R. D. (1992) *Rev. Sci. Instrum. 63*, 2187–2192.

Tang, X.-S., Diner, B. A., Larsen, B. S., Gilchrist, M. L., Lorigan, G. A., & Britt, R. D. (1994) *Proc. Natl. Acad. Sci. U.S.A. 91*, 704–708.

Van Vleck, J. H. (1940) *Phys. Rev. 57*, 426–447.

Weil, J. A., Bolten, J. R., & Wertz, J. E. (1994) *Electron Paramagnetic Resonance*, Wiley, New York.

Zimmermann, J.-L., & Rutherford, A. W. (1984) *Biochim. Biophys. Acta 767*, 160–167.

Zimmerman, J.-L., & Rutherford, A. W. (1986) *Biochemistry 25*, 4609–4615.